Chapter 2
Detection of Parametric Roll for Ships

Roberto Galeazzi, Mogens Blanke, and Niels K. Poulsen

2.1 Introduction

Observations of parametric resonance on ships were first done by Froude [9, 10] who reported that a vessel, whose frequency of oscillation in heave/pitch is twice its natural frequency in roll, shows undesirable seakeeping characteristics that can lead to the possibility of exciting large roll oscillations. Theoretical explanations appeared in the 20th century, see [26, 35] and references herein, and parametrically induced roll has been a subject in maritime research since the early 1950s [23] and [32]. The report by France et al. [8] about the *APL China* incident in October 1998 accelerated the awareness and parametric roll resonance became an issue of key concern. Døhlie [7] emphasized parametric resonance as a very concrete phenomenon, which will be able to threaten some of the giants of the sea in common passage conditions, which were previously considered to be of no danger.

Publications addressing parametric roll on container ships include [3,5,17,20,21, 24,33,34,36]. Fishing vessels were in focus in [27,28]. A main topic of this research has been to analyse the nonlinear interactions between roll and other ships' motions and develop models, which could predict vessels' susceptibility to parametric roll at the design stage. However, commercial interest is to maximize cargo capacity.

R. Galeazzi (✉) • M. Blanke
Department of Electrical Engineering, Technical University of Denmark, DTU Electrical Engineering, DK 2800 Kgs. Lyngby, Denmark

Center for Ships and Ocean Structures, Norwegian University of Science and Technology, NO-7491 Trondheim, Norway
e-mail: rg@elektro.dtu.dk; mb@elektro.dtu.dk

N.K. Poulsen
Department of Electrical Engineering, Technical University of Denmark, DTU Informatics, 2800 Lyngby, Denmark
e-mail: nkp@imm.dtu.dk

T.I. Fossen and H. Nijmeijer (eds.), *Parametric Resonance in Dynamical Systems*,
DOI 10.1007/978-1-4614-1043-0_2, © Springer Science+Business Media, LLC 2012

Hull designs have not been significantly changed and parametric resonance is left as a calculated risk. Therefore, there is a need to enhance safety against parametric roll through on-board detection and decision support systems.

First generation warning systems are based on longer horizon analysis of ship's responses and they provide polar diagrams with risk zones in speed and heading. These are found in commercial products as the SeaSense [30] and the Amarcon's OCTOPUS Resonance.[1] For detection of the resonant bifurcation mode, Holden et al. [19] proposed an observer based predictor that estimates the eigenvalues of a linear second-order oscillatory system. This algorithm issues a warning when eigenvalues have positive real parts. The method works convincingly but was designed to cope with excitation by narrow band regular waves. Irregular sea conditions were studied by McCue and Bulian [25] who used finite time Lyapunov exponents to detect the onset of parametric roll, but this method was not found to possess sufficiently robustness when validated against experimental data.

Starting from early results outlined in [12,13] this chapter re-visits the core of the theory of parametric resonance and proposes signal-based methods for detection of parametric roll [11]. Development of a robust warning system for detecting the onset of parametric roll is discussed, and it is shown possible to obtain based solely on signals. The core of the method is shown to consist of two detection schemes: one in the frequency domain, a second in the time domain. The frequency-based detector uses an indicator of spectral correlation between pitch or heave and the roll. A time-based detector exploits the phase synchronization between the square of the roll and of pitch. A generalized likelihood ratio test (GLRT) is derived for a Weibull distribution that is observed from data and adaptation is employed to obtain robustness in reality with time-varying weather conditions. Robustness to forced roll motion is also discussed and the detection system's performance is evaluated on two data sets: model test data from towing tank experiments and data from a container vessel experiencing an Atlantic storm.

2.2 Parametric Roll – Conditions and Underlying Physics

This section presents empirical experience and introduces a mathematical treatment of parametric roll resonance.

2.2.1 Empirical Conditions

Empirical conditions have been identified that may trigger parametric roll resonance:

[1] http://www.amarcon.com

1. the period of the encounter wave is approximately equal to half the roll natural period ($T_e \approx \frac{1}{2} T_\phi$)
2. the wave length is approximately equal to the ship's length ($\lambda_w \approx L_{PP}$)
3. the wave height is greater than a ship-dependent threshold ($h_w > \bar{h}_s$)

When these conditions are met, and the ship sails in moderate to heavy longitudinal or oblique seas, then the wave passage along the hull and the wave excited vertical motions result in variations of the intercepted water-plane area and in turn, they change the roll restoring characteristics. The onset of parametric resonance causes a quick rise of roll oscillation, which can reach amplitudes larger than $\pm 40^\circ$ ([6, 8]), and it may bring the vessel into conditions dangerous for cargo, crew, and hull integrity. Damages produced by parametric roll to the post-Panamax container ship *APL China* had a price tag of USD 50 millions in 1998 [15].

2.2.2 Mathematical Background

Consider a vessel sailing in moderate head regular seas and let the wave elevation be modeled as a single frequency sinusoid

$$\zeta(t) = A_w \cos(kx \cos\chi - ky \sin\chi - \omega_e t),$$

where A_w is the wave amplitude, ω_e the wave encounter frequency, k the wave number, and χ the wave encounter angle. In head seas the wave encounter angle is $\chi = 180^\circ$, and

$$\zeta(t) = A_w \cos(kx + \omega_e t).$$

The incident wave gives rise to forces and moments acting on the hull. In head seas, conventional forced roll cannot occur since forces and moments from wave pressure on the hull have no components perpendicular to the ship, but motions in the vertical plane are clearly excited. Heaving and pitching cause periodic variations of the submerged hull geometry. In particular, during a wave passage, the intercepted water-plane area S_w changes from the still water case S_{w_0}, causing a variation of the position of the center of buoyancy [29]. This in turn gives rise to a modification of the transverse metacentric height GM and also to a new position of the metacenter M. The center of gravity G depends upon the ship's loading condition and is fixed. Consequently the periodic fluctuation of GM, which can be considered sinusoidal,

$$\mathrm{GM}(t) = \overline{\mathrm{GM}} + \mathrm{GM}_a \cos(\omega_e t)$$

influences the stability properties of the vessel through the roll restoring moment that is approximated by:

$$\tau(t) \approx \rho g \nabla \mathrm{GM}(t) \sin\phi,$$

where $\overline{\mathrm{GM}}$ is the mean value of the metacentric height, $\mathrm{GM_a}$ is the amplitude of the variations of the metacentric height in waves, ρ is the water density, g is the acceleration constant of gravity, and ∇ is the displaced volume.

The following situations alternate in a periodic manner:

- a wave trough is amidships: in this case $S_\mathrm{W} > S_{\mathrm{W}_0}$ causing a larger restoring moment ($\tau > \tau_0$) and increased stability
- a wave crest is amidships: in this case $S_\mathrm{W} < S_{\mathrm{W}_0}$ inducing a smaller restoring moment ($\tau < \tau_0$) and reduced stability.

If a disturbance occurs in roll when the ship is between the wave crest and trough at amidships position, then its response will be greater than in calm water since it is approaching a situation of instantaneous increased stability. Therefore the vessel will roll back to a larger angle than it would have done in calm water. After the first quarter of the roll period T_ϕ the vessel has rolled back to the zero degree attitude but it continues towards port side due to the inertia. However now the ship encounters a wave crest amidships, which determines a reduced restoring moment with respect to that in calm water; therefore the ship rolls to a larger angle than it would have done in calm water. As a result the roll angle is increased again over the second quarter of the roll period, reaching a higher value than at the end of the first quarter. This alternate sequence of instantaneous increased and reduced restoring moment causes the roll angle to keep increasing unless some other factors start counteracting it.

Formally, this can be described as the interaction between coupled modes of an autoparametric system, where the primary system is externally forced by a sinusoidal excitation. In particular, let θ be the pitch angle, and ϕ be the roll angle. Then the system reads

$$\left(I_y - M_{\ddot{\theta}}\right)\ddot{\theta} + M_{\dot{\theta}}\dot{\theta} + M_\theta\theta + M_{\phi^2}\phi^2 = M_\mathrm{w}\cos(\omega_\mathrm{w}t), \tag{2.1}$$

$$\left(I_x - K_{\ddot{\phi}}\right)\ddot{\phi} + K_{\dot{\phi}}\dot{\phi} + K_\phi\phi + K_{\phi^3}\phi^3 + K_{\phi\theta}\phi\theta = 0, \tag{2.2}$$

where I_x, I_y are the rigid body inertia in roll and pitch; $K_{\ddot{\phi}}$, $M_{\ddot{\theta}}$ are the added inertia; $K_{\dot{\phi}}$, $M_{\dot{\theta}}$ are the linear damping due to viscous effects; K_ϕ, K_{ϕ^3}, $K_{\phi\theta}$, M_θ, and M_{ϕ^2} are the linear and the nonlinear coefficients of the restoring moments due to hydrostatic actions; M_w, ω_w are the amplitude and frequency of the wave induced pitch moment. The model introduced above is not meant to precisely describe the hull–wave interactions that determine the onset and development of parametric roll on ships, but it simply tries to cast the roll–pitch dynamics within the autoparametric resonance framework along the lines of [31].

System (2.1)–(2.2) can be rewritten as:

$$\ddot{\theta} + \mu_1\dot{\theta} + \omega_1^2\theta + \alpha_1\phi^2 = \kappa\cos(\omega_\mathrm{w}t) \tag{2.3}$$

$$\ddot{\phi} + \mu_2\dot{\phi} + \omega_2^2\phi + \varepsilon\phi^3 + \alpha_2\phi\theta = 0 \tag{2.4}$$

with coefficients

$$\mu_1 = \frac{M_{\dot{\theta}}}{I_y - M_{\ddot{\theta}}}\,,\ \omega_1 = \sqrt{\frac{M_{\theta}}{I_y - M_{\ddot{\theta}}}}\,,\ \alpha_1 = \frac{M_{\phi^2}}{I_y - M_{\ddot{\theta}}}\,,\ \kappa = \frac{M_{\mathrm{w}}}{I_y - M_{\ddot{\theta}}}$$

$$\mu_2 = \frac{K_{\dot{\phi}}}{I_x - K_{\ddot{\phi}}}\,,\ \omega_2 = \sqrt{\frac{K_{\phi}}{I_x - K_{\ddot{\phi}}}}\,,\ \alpha_2 = \frac{K_{\phi\theta}}{I_x - K_{\ddot{\phi}}}\,,\ \varepsilon = \frac{K_{\phi^3}}{I_x - K_{\ddot{\phi}}}\,.$$

The so-called *semi-trivial* solution of the system (2.3)–(2.4) can be determined by posing

$$\theta(t) = \theta_0 \cos(\omega_{\mathrm{w}} t + \varsigma) \tag{2.5}$$

$$\phi(t) = 0 \tag{2.6}$$

and by substituting $\theta(t)$ and $\phi(t)$ into (2.3) and (2.4) it yields

$$\theta_0 = \frac{\kappa}{\sqrt{\left(\omega_1^2 - \omega_{\mathrm{w}}^2\right)^2 + \mu_1^2 \omega_{\mathrm{w}}^2}}. \tag{2.7}$$

The stability of the semi-trivial solution is investigated by looking at its behavior in a neighborhood defined as:

$$\theta(t) = \theta_0 \cos(\omega_{\mathrm{w}} t + \varsigma) + \delta_\theta(t), \tag{2.8}$$

$$\phi(t) = 0 + \delta_\phi(t), \tag{2.9}$$

where δ_θ and δ_ϕ are small perturbations. Substituting (2.8) and (2.9) into the system (2.3)–(2.4), and linearizing about the semi-trivial solution the following system is obtained

$$\ddot{\delta}_\theta + \mu_1 \dot{\delta}_\theta + \omega_1^2 \delta_\theta = 0 \tag{2.10}$$

$$\ddot{\delta}_\phi + \mu_2 \dot{\delta}_\phi + \left(\omega_2^2 + \alpha_2 \theta_0 \cos\left(\omega_{\mathrm{w}} t + \varsigma\right)\right) \delta_\phi = 0. \tag{2.11}$$

Equation (2.10) has the solution $\delta_\theta = 0$, which is exponentially stable since $\mu_1 > 0$. Therefore, the stability of the semi-trivial solution is fully determined by (2.11), which is referred to as the damped Mathieu equation. By applying Floquet theory [16] it is possible to show that (2.11) has its principal instability region for $\omega_2 \approx \frac{1}{2}\omega_{\mathrm{w}}$, and its boundary is given by:

$$\frac{1}{4}\frac{\mu_2^2}{\omega_{\mathrm{w}}^2} + \left(\frac{\omega_2^2}{\omega_{\mathrm{w}}^2} - \frac{1}{4}\right)^2 = \frac{1}{4}\frac{\alpha_2^2 \theta_0^2}{\omega_{\mathrm{w}}^4}. \tag{2.12}$$

This boundary condition can be used to determine the critical value κ_c of the external excitation, which triggers the parametric resonance in the secondary system. In particular substituting (2.7) into (2.12) we obtain

$$\kappa_c = 2\frac{\omega_w^2\sqrt{\left(\omega_1^2-\omega_w^2\right)^2+\mu_1^2\omega_w^2}}{\alpha_2}\sqrt{\frac{1}{4}\frac{\mu_2^2}{\omega_w^2}+\left(\frac{\omega_2^2}{\omega_w^2}-\frac{1}{4}\right)^2}. \tag{2.13}$$

For $\kappa > \kappa_c$ the semi-trivial solution becomes unstable, and a nontrivial solution appears which is given by:

$$\theta(t) = \theta_1\cos(\omega_w t+\varsigma_1), \tag{2.14}$$

$$\phi(t) = \phi_0\cos\left(\frac{1}{2}\omega_w t+\varsigma_2\right), \tag{2.15}$$

where

$$\theta_1 = \frac{2\omega_w^2}{\alpha_2}\sqrt{\frac{1}{4}\frac{\mu_2^2}{\omega_w^2}+\left(\frac{\omega_2^2}{\omega_w^2}-\frac{1}{4}\right)^2} \tag{2.16}$$

and ϕ_0 grows over time.

The system (2.3)–(2.4) shows a saturation phenomenon both in pitch and in roll. For values of the excitation amplitudes between 0 and κ_c the semi-trivial solution is hence stable with an amplitude that grows linearly with κ, as shown in (2.7). When the amplitude of the external excitation becomes larger than κ_c then the semi-trivial solution loses stability and a nontrivial solution appears. In particular (2.16) shows that the amplitude of the solution of the primary system stays constant, whereas the amplitude of the secondary system grows with increasing κ. Therefore, when the excitation amplitude increases, the amount of energy stored in the primary system stays constant and the entire energy rise flows to the secondary system. The rate at which energy is pumped into the secondary system is not constant but varies according to the change of the phase ς_2, which is connected to the variation of the amplitude ϕ_0 through the nonlinearity in the restoring moment. When the rate at which energy being dissipated by viscous effects has matched the rate at which energy is transferred to the roll subsystem, the system reaches a steady state motion characterized by a constant amplitude ϕ_0 and a phase shift $\varsigma_2 = \pi$. Figure 2.1 shows the development of parametric roll resonance while the amplitude of the excitation $\bar{\kappa} = \kappa/\kappa_c$ increases: the stability chart clearly illustrates in the parameter space how the stability properties of the secondary system changes in response to a variation of the amplitude of the external excitation.

Concluding, parametric roll is a resonance phenomenon triggered by existence of the frequency coupling $\omega_w \approx 2\omega_2$, and whose response shows a phase synchronization of 180° with the parametric excitation.

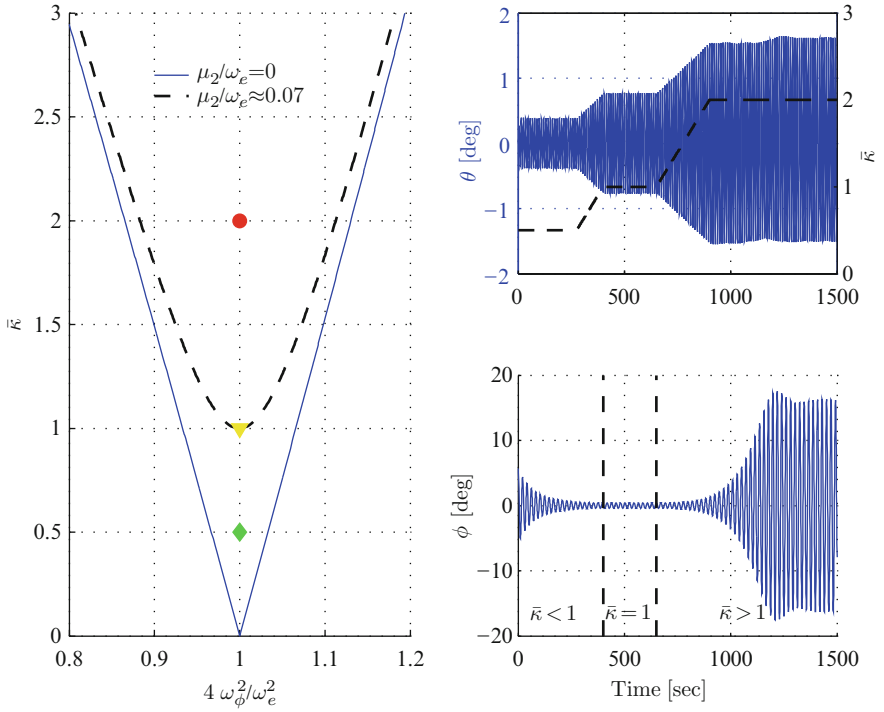

Fig. 2.1 Parametric resonance in the pitch–roll auto-parametric system: (*left*) stability diagram of the secondary system for different levels of damping, and different amplitude of the excitation; (*right*) pitch and roll time series evolution

2.3 Detection Methods

Change detection is often based on a statistical test between a hypothesis $\mathscr{H}_0$ and an alternative $\mathscr{H}_1$. The hypothesis $\mathscr{H}_0$ is related to the normal situation whereas the alternative is related to a deviation from normal.

Assume the data available for the test are $\mathbf{Y} = [y(1), \ldots, y(N)]$, and that it is possible to assign a distribution of the data for the normal (fault free) case $p(\mathbf{Y}; \mathscr{H}_0)$ and for the not-normal (faulty) case $p(\mathbf{Y}; \mathscr{H}_1)$, as shown in Fig. 2.2.

Applying the Neyman–Pearson strategy (see, e.g., [2, 22] or [4]) $\mathscr{H}_1$ will be decided if

$$L(\mathbf{Y}) = \frac{p(\mathbf{Y}; \mathscr{H}_1)}{p(\mathbf{Y}; \mathscr{H}_0)} > \gamma, \tag{2.17}$$

where γ is a design parameter. The function $L(\mathbf{Y})$ is referred to as the likelihood ratio. Then the detection process can be seen as a mapping from a data manifold

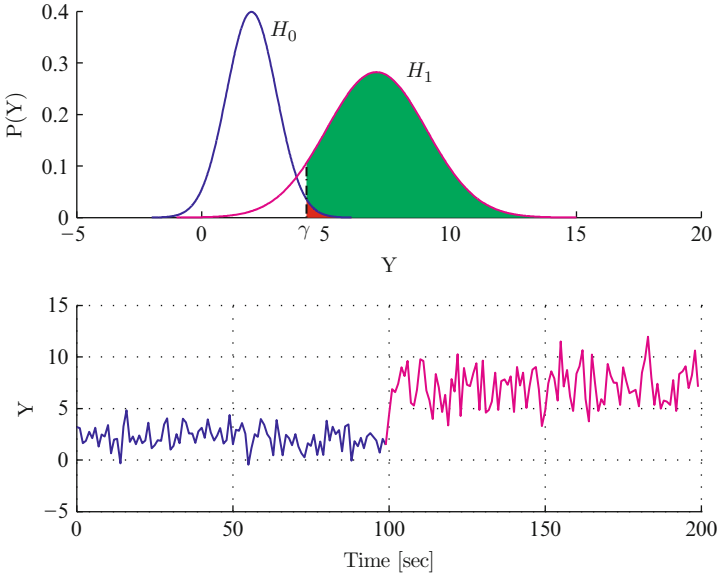

Fig. 2.2 *Top*: Distributions of data in the fault free case $\mathscr{H}_0$ and in the faulty case $\mathscr{H}_1$. *Bottom*: Data when a fault occur at $t = 100$

into a decision manifold. When testing between two simple hypothesis the decision manifold is divided into two regions defined as:

$$R_0 = \{\mathbf{Y} : \text{ decide } \mathscr{H}_0 \text{ or reject } \mathscr{H}_1\}$$
$$R_1 = \{\mathbf{Y} : \text{ decide } \mathscr{H}_1 \text{ or reject } \mathscr{H}_0\},$$

where R_1 is called the critical region.

Performing a statistical test, two types of erroneous decisions can be made. A false alarm if deciding $\mathscr{H}_1$ while $\mathscr{H}_0$ is true, or a missed detection if deciding $\mathscr{H}_0$ while $\mathscr{H}_1$ is true.

While $\mathscr{H}_1$ true, the probability of false alarm is $P_{\text{FA}} = P(\mathscr{H}_1; \mathscr{H}_0)$ and the probability of correct detection is $P_{\text{D}} = P(\mathscr{H}_1; \mathscr{H}_1)$. Both depend on the threshold γ chosen, as illustrated in Fig. 2.2. In a simple test situation (the distribution of data is known in both the normal and in the faulty situation) the Neyman–Pearson test in (2.17) maximizes P_{D} for a given P_{FA}.

In the composite situation, where the two distributions are not precisely known, but they depend on some unknown parameters, the generalized likelihood ratio test results in deciding $\mathscr{H}_1$ if

$$L(\mathbf{Y}) = \frac{p(\mathbf{Y}; \hat{\theta}_1, \mathscr{H}_1)}{p(\mathbf{Y}; \hat{\theta}_0, \mathscr{H}_0)} > \gamma, \tag{2.18}$$

where $\hat{\theta}_i$ is the maximum likelihood estimate (MLE) of θ_i, i.e.,

$$\hat{\theta}_i = \max_{\theta} L(\mathbf{Y}|\theta_i; \mathscr{H}_i) \,. \tag{2.19}$$

The specific detection methods that follow below are patent pending [11].

2.3.1 Detection in the Frequency Domain

In Sect. 2.2 it was shown that the onset and development of parametric roll is attributable to the transfer of energy from the pitch mode (but also heave motion can contribute), directly excited by the wave motion, to the roll mode, at a frequency about twice the natural roll frequency. Therefore, an increase of power of roll square close to the frequencies where pitch is pumping energy into roll may be exploited as an indicator of parametric resonance.

Given two signals, e.g., $x(t)$ and $y(t)$, the cross-correlation provides a measure of similarity of the two waveforms as a function of time lag. If the two signals are discrete sequences then the cross-correlation and cross-spectrum are defined as:

$$\begin{aligned} r_{xy}[m] &\triangleq \sum_{m=-\infty}^{\infty} x^*[m]y[n+m], \\ P_{xy}(\omega) &\triangleq \sum_{m=-\infty}^{\infty} r_{xy}[m]e^{-j\omega m}, \end{aligned} \tag{2.20}$$

where m is the time lag, and * denotes complex conjugate. The functions carry information about which components are held in common between the two signals and since it is the roll sub-harmonic regime addressing the onset of parametric roll resonance, the detection problem can be set up as monitoring the cross-spectrum of $\phi^2[n]$ and $\theta[n]$.

The parametric roll detection problem is then formulated as:

$$\begin{aligned} \mathscr{H}_0 &: P_{\phi^2\theta}(\omega) \leq \bar{P}, \\ \mathscr{H}_1 &: P_{\phi^2\theta}(\omega) > \bar{P}, \end{aligned} \tag{2.21}$$

where $\bar{P}$ is a power threshold. Instead of using directly the cross-spectrum, a spectral correlation coefficient could be exploited, defined as:

$$\mathscr{S}_{\phi^2\theta} \triangleq \frac{\sigma^2_{\phi^2\theta}}{\sqrt{\sigma^2_{\phi^2}\sigma^2_{\theta}}}. \tag{2.22}$$

where $\sigma^2_{\phi^2\theta}$ is the average power of the cross-spectrum of ϕ^2 and θ, $\sigma^2_{\phi^2}$ is the average power of the square of the roll angle, and σ^2_{θ} is the average power of the pitch angle.

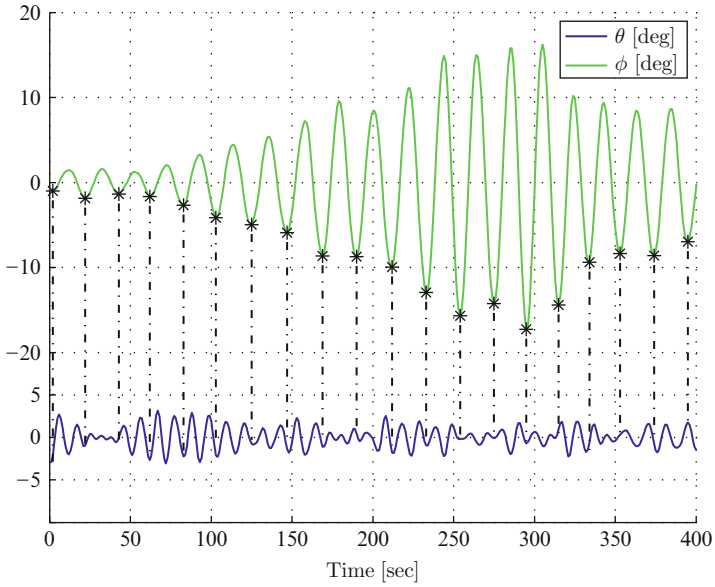

Fig. 2.3 Model tank experiment 1195: alignment of peaks between pitch θ and roll ϕ during the onset and development of parametric roll

The detection problem can then be rewritten as:

$$\begin{aligned} \mathscr{H}_0 &: \mathscr{S}_{\phi^2\theta} \leq \bar{\mathscr{S}}, \\ \mathscr{H}_1 &: \mathscr{S}_{\phi^2\theta} > \bar{\mathscr{S}}, \end{aligned} \tag{2.23}$$

where $\bar{\mathscr{S}}$ is a measure of the level of spectral correlation.

2.3.2 Detection in the Time Domain

2.3.2.1 Statistics of the Driving Signal

After onset, parametric roll resonance is characterized by nonlinear synchronization between motions. Døhlie [7] pointed out that when parametric roll develops there is a lining up of peaks between the pitch motion and the roll motion, that is, every second peak of pitch is in-phase with the peak in roll, as shown in Fig. 2.3. Figure 2.3 also shows that when this alignment is partially lost, the roll oscillations start decaying, as e.g., between 150 s and 250 s, or after 300 s. Therefore, a signal which carries the phase information of pitch and roll could be exploited for solving the detection problem.

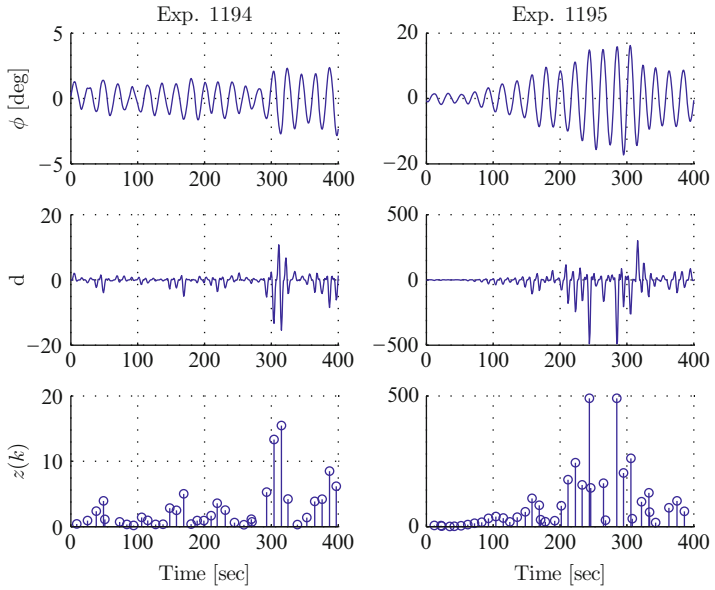

Fig. 2.4 Negative and positive peaks in d address how the amplitude of the roll oscillations increases and decreases. Data from model basin test

Following [13], given the roll angle ϕ and the pitch angle θ, the signal indicating the parametric resonance in roll is defined as:

$$d(t) \triangleq \lambda(t)\phi^2(t)\theta(t), \tag{2.24}$$

where the time-varying scaling factor $0 < \lambda(t) \leq 1$ is introduced to reduce the sensitivity to variations in sea state. Consider Fig. 2.4, where $\phi(t)$ and $d(t)$ are plotted for one experiment without parametric roll (Exp. 1194) and another with parametric roll (Exp. 1195). The *driving* signal $d(t)$ characterizes quite well the way the amplitude grows or decays inside the signal ϕ. When the amplitude of ϕ abruptly grows, a sequence of negative spikes shows up in the driving signal. In contrast, when the amplitude of ϕ decreases, positive spikes reflect this in $d(t)$.

Moreover, when parametric roll is developing, the magnitudes of the negative spikes in the driving signal are much larger than that seen when the roll mode is not in a resonant condition (Fig. 2.4, middle plots). Therefore, a significant variation in the variance of the driving signal $d(t)$ can be expected when parametric roll is developing. An alternative to directly using the $d(t)$ signal would be to use the amplitude of local minima between up-crossings,

$$z(k) \triangleq -\min(d(t)), \quad t \in]T(k-1), T(k)], \tag{2.25}$$

where $T(k)$ are the time-tags of up-crossings in $d(t)$.

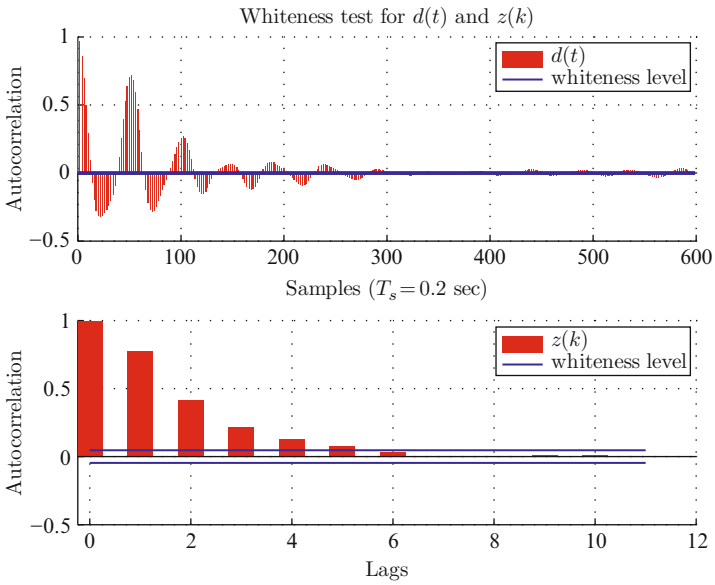

Fig. 2.5 Auto-correlation of driving signal $d(t)$ and local minima $z(k)$. Data from Atlantic passage during a storm

An important condition for subsequent statistical testing and correct selection of thresholds, is that data are independent and identically distributed (IID). A plot of the autocorrelation functions of $d(t)$ and $z(k)$ under the hypothesis $\mathscr{H}_0$ is shown in Fig. 2.5. The driving signal $d(t)$ is heavily correlated due to the narrow-band process that creates this signal. The autocorrelation of the local minima $z(k)$ have a smooth roll-off with a forgetting factor of 0.3. If whitening of $z(k)$ should subsequently be needed, a simple discrete filter could be employed for this purpose. The autocorrelation behavior makes $z(k)$ a natural choice for subsequent statistical analysis in the time-domain.

As to the distribution of $z(k)$, a scrutiny showed that a Weibull distribution characterizes $z(k)$ quite well. The Weibull distribution, which is defined only for $z > 0$, has cumulative density function, CDF:

$$P(z) = 1 - \exp\left(-\left(\frac{z}{\upsilon}\right)^{\beta}\right) \tag{2.26}$$

and probability density function, PDF:

$$p(z) = \frac{\beta}{2\upsilon^{\beta}}(z)^{\beta-1}\exp\left(-\left(\frac{z}{\upsilon}\right)^{\beta}\right), \tag{2.27}$$

where υ and β are scale and shape parameters, respectively.

According to the observations from model test data, a good way to discriminate between resonant and nonresonant cases is to look for a variation in signal power. In particular, the bottom plots of Fig. 2.4 show that the onset of parametric resonance in roll is preceded by an abrupt variation of the amplitude of $z(k)$; therefore, a detector which looks for large changes in signal power is aimed at. For the Weibull distribution the variance is given by:

$$\sigma^2 = \upsilon^2 \left[\Gamma\left(1+\frac{2}{\beta}\right) - \Gamma^2\left(1+\frac{1}{\beta}\right) \right].$$

Hence the detection scheme must trail variations in scale and shape parameters.

2.3.2.2 GLRT for Weibull Processes ($\mathscr{W}$-GLRT)

Assume that the local minima $z(t)$ of the driving signal is a realization of a Weibull random process. Then the distribution of N independent and identically distributed samples of z is characterized by the probability density function:

$$\mathscr{W}(\mathbf{z};\theta) = \left(\frac{\beta}{2\upsilon^\beta}\right)^N \prod_{k=0}^{N-1} \left[z_k^{\beta-1} \exp\left(-\left(\frac{z_k}{\upsilon}\right)^\beta \right) \right], \tag{2.28}$$

where $\theta = [\upsilon, \beta]^T$ is the parameter vector fully describing the Weibull PDF.

The detection of parametric roll can be formulated as a parameter test of the probability density function:

$$\begin{aligned} \mathscr{H}_0 &: \theta = \theta_0, \\ \mathscr{H}_1 &: \theta = \theta_1, \end{aligned} \tag{2.29}$$

where θ_0 is known and it represents $\mathscr{W}$ in the nonresonant case, whereas θ_1 is unknown and it describes the parametric resonant case. By applying the generalized likelihood ratio test, the detector decides $\mathscr{H}_1$ if

$$L_G(\mathbf{z}) = \frac{p\left(\mathbf{z};\hat{\theta}_1,\mathscr{H}_1\right)}{p\left(\mathbf{z};\theta_0,\mathscr{H}_0\right)} > \gamma, \tag{2.30}$$

where the unknown parameter vector θ_1 is replaced with its maximum likelihood estimate $\hat{\theta}_1$, and γ is the threshold given by the desired probability of false alarms.

The first step in computing L_G is to determine $\hat{\theta}_1 = \left[\hat{\upsilon}_1, \hat{\beta}_1\right]^T$, therefore we need to maximize $p\left(\mathbf{z};\hat{\theta}_1,\mathscr{H}_1\right)$. Given $p\left(\mathbf{z};\hat{\theta}_1\right)$ the estimates of the parameters υ_1 and β_1 are computed as:

$$\frac{\partial \ln p\left(\mathbf{z};\hat{\theta}_1\right)}{\partial \theta_j} = 0$$

which results in

$$\hat{\upsilon}_1 = \left(\frac{1}{N} \sum_{k=0}^{N-1} z_k^{\hat{\beta}_1} \right)^{\frac{1}{\hat{\beta}_1}} \tag{2.31}$$

$$\frac{1}{\hat{\beta}_1} = \frac{\sum_{k=0}^{N-1} z_k^{\hat{\beta}_1} \ln z_k}{\sum_{k=0}^{N-1} z_k^{\hat{\beta}_1}} - \frac{1}{N} \sum_{k=0}^{N-1} \ln z_k \ . \tag{2.32}$$

Balakrishnan and Kateri [1] have shown that $\hat{\beta}_1$ exists, it is unique, and its value is given by the intersection of the curve $1/\hat{\beta}_1$ with the right-hand side of (2.32).

Having determined the MLEs $\hat{\upsilon}_1$ and $\hat{\beta}_1$ it is then possible to derive an explicit form for the detector. By taking the natural logarithm of both sides of (2.30),

$$\ln \frac{\left(\frac{\beta_1}{2\upsilon_1^{\beta_1}} \right)^N \prod_{k=0}^{N-1} \left[z_k^{\beta_1 - 1} \exp\left(- \left(\frac{z_k}{\upsilon_1} \right)^{\beta_1} \right) \right]}{\left(\frac{\beta_0}{2\upsilon_0^{\beta_0}} \right)^N \prod_{k=0}^{N-1} \left[z_k^{\beta_0 - 1} \exp\left(- \left(\frac{z_k}{\upsilon_0} \right)^{\beta_0} \right) \right]} > \ln \gamma \Rightarrow$$

$$N \ln \left(\frac{\beta_1}{\beta_0} \frac{\upsilon_0^{\beta_0}}{\upsilon_1^{\beta_1}} \right) + (\beta_1 - \beta_0) \sum_{k=0}^{N-1} \ln z_k - \sum_{k=0}^{N-1} \left(\frac{z_k}{\upsilon_1} \right)^{\beta_1} + \sum_{k=0}^{N-1} \left(\frac{z_k}{\upsilon_0} \right)^{\beta_0} > \ln \gamma, \tag{2.33}$$

where the parameters $[\beta_1, \upsilon_1]$ are replaced by their estimates.

Data show that the shape parameter is approximately the same under both hypothesis, $\beta_1 = \beta_0 = \beta$, then the GLRT reads

$$N\beta \ln \left(\frac{\upsilon_0}{\hat{\upsilon}_1} \right) + \frac{\hat{\upsilon}_1^{\beta} - \upsilon_0^{\beta}}{(\upsilon_0 \hat{\upsilon}_1)^{\beta}} \sum_{k=0}^{N-1} z_k^{\beta} > \ln \gamma \Rightarrow$$

$$N\beta \ln \left(\frac{\upsilon_0}{\hat{\upsilon}_1} \right) + N \frac{\hat{\upsilon}_1^{\beta} - \upsilon_0^{\beta}}{\upsilon_0^{\beta}} > \ln \gamma. \tag{2.34}$$

Therefore the test quantity $g(k)$ is

$$g(k) = \left(\frac{\hat{\upsilon}_1(k)}{\upsilon_0} \right)^{\beta} - 1 - \beta \ln \left(\frac{\hat{\upsilon}_1(k)}{\upsilon_0} \right) \tag{2.35}$$

and the threshold where $\mathscr{H}_1$ is decided is

$$g(k) > \frac{\ln \gamma}{N} \equiv \gamma_g. \tag{2.36}$$

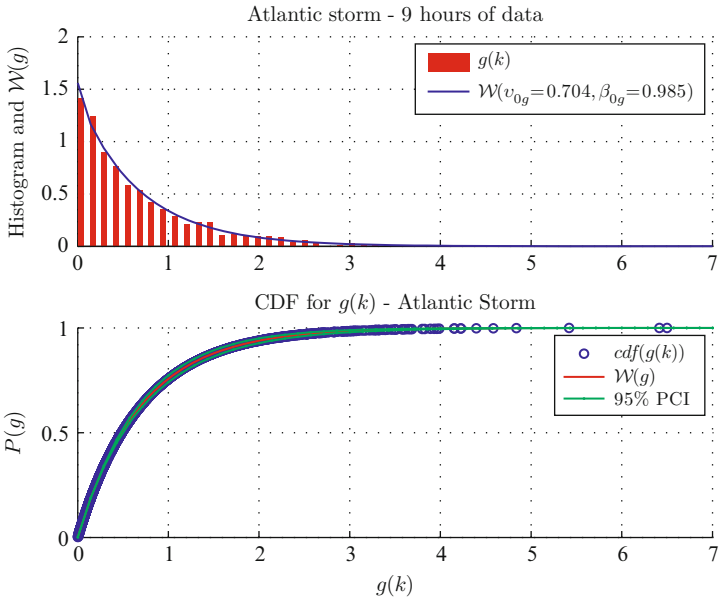

Fig. 2.6 Test statistics $g(k)$ observed in heavy weather conditions with forced roll. Data from Atlantic passage during a storm. A Weibull distribution fits the data well

Asymptotically, as $N \to \infty$ a theoretical value exists for γ, independent of distribution of $z(k)$. However, since only few peaks are used here, the distribution of $g(k)$ need be investigated and the value of the threshold γ_g need be determined from this distribution.

2.3.2.3 Selection of Threshold

Selection of the threshold γ_g to obtain a sufficiently low false alarm rate, depends on the statistics of $g(k)$ in (2.35) under assumption $\mathscr{H}_0$. Given the test signal $g(k)$, which behaves according to the PDF $p(g;\mathscr{H}_0)$ under the hypothesis $\mathscr{H}_0$, the threshold γ_g, which obtains a given false alarm probability, follows from

$$P_{\text{FA}} = \int_{\{g:L_G(g)>\gamma_g\}} p\,(g;\mathscr{H}_0)\,\mathrm{d}g. \tag{2.37}$$

Since the GLRT runs over only few peaks to obtain rapid detection, asymptotic results for the distribution of $g(k)$ are not applicable. Instead, the distribution $p(g;\mathscr{H}_0)$ can be reliably estimated from data. A plot of the histogram of the test statistics $g(k)$ is shown in Fig. 2.6 together with the estimated Weibull distribution. The data used are recordings from a container vessel during 9 h of navigation through an Atlantic storm.

Having obtained the parameters υ_{0g} and β_{0g} of the Weibull distribution for $g(k)$ under $\mathscr{H}_0$, $\mathscr{W}(g(k);\mathscr{H}_0)$, the threshold for a desired false alarm probability is obtained from

$$1 - P_{\mathrm{FA}} = 1 - \exp\left(-\left(\frac{\gamma_g}{\upsilon_{0g}}\right)^{\beta_{0g}}\right) \tag{2.38}$$

or

$$\gamma_g = \upsilon_{0g}\left(-\ln P_{\mathrm{FA}}\right)^{\frac{1}{\beta_{0g}}}. \tag{2.39}$$

For the hypothesis $\mathscr{H}_0$ shown in Fig. 2.6 the Weibull fit is characterized by $\upsilon_0 = 0.70 \pm 0.04$ and $\beta_0 = 0.99 \pm 0.04$; hence to obtain a probability of false alarms $P_{\mathrm{FA}} = 0.0001$, the threshold must be set to $\gamma_g = 5.0$.

2.3.2.4 Robustness Against Forced Roll

For a real ship sailing in oblique short-crested seaways some forced roll with frequency equal to the encounter frequency will always occur. This does not obscure the proposed detection schemes since both the spectral correlation coefficient and the GLRT for nonGaussian processes are insensitive to forced roll.

Consider pitch and roll as narrow-band signals:

$$\theta(t) \text{ s.t. } \Theta(\omega) = 0 \text{ for } |\omega - \omega_\theta| \geq \Omega_\theta,$$
$$\phi(t) \text{ s.t. } \Phi(\omega) = 0 \text{ for } |\omega - \omega_\phi| \geq \Omega_\phi,$$

where $\Theta(\omega)$ and $\Phi(\omega)$ are the spectra of pitch and roll centered at the center frequency ω_θ and ω_ϕ respectively. The bands of the spectra are given by $B_\theta = \{\omega \text{ s.t. } |\omega - \omega_\theta| < \Omega_\theta\}$ and $B_\phi = \{\omega \text{ s.t. } |\omega - \omega_\phi| < \Omega_\phi\}$, where $W_\theta = 2\Omega_\theta$ and $W_\phi = 2\Omega_\phi$ are the bandwidths.

If $\omega_\theta = \omega_e = 2\omega_\phi$, as in parametric resonance, then $B_\theta = \{\omega \text{ s.t. } |\omega - 2\omega_\phi| < \Omega_\theta\}$, hence the spectrum of the square of the roll angle overlaps in large part or completely the pitch spectrum. With pitch and the roll signals:

$$\theta(t) = \theta_0(t)\cos(2\omega_\phi t + \psi_\theta(t)) \tag{2.40}$$
$$\phi(t) = \phi_0(t)\cos(\omega_\phi t + \psi_\phi(t)) \tag{2.41}$$

the spectra of pitch and of the square of roll are

$$\begin{aligned}\Theta(\omega) = \frac{1}{2}\big[&\Theta_i(\omega-2\omega_\phi)+\Theta_i(\omega+2\omega_\phi)\\ &-\Theta_q(\omega-2\omega_\phi)-\Theta_q(\omega+2\omega_\phi)\big] \qquad (2.42)\\ \Phi_2(\omega) = \frac{1}{2}\big[&\Phi_0(\omega)+\Phi_i(\omega-2\omega_\phi)+\Phi_i(\omega+2\omega_\phi)\\ &-\Phi_q(\omega-2\omega_\phi)-\Phi_q(\omega+2\omega_\phi)\big]. \qquad (2.43)\end{aligned}$$

Here $\Theta_i = \mathscr{F}(\theta_0(t)\cos(\psi_\theta(t)))$, and $\Theta_q = \mathscr{F}(\theta_0(t)\sin(\psi_\theta(t)))$ are the Fourier transforms of the in-phase and quadrature components of the pitch angle; whereas $\Phi_0 = \mathscr{F}(\phi_0^2(t))$, $\Phi_i = \mathscr{F}(\phi_0^2(t)\cos(2\psi_\phi(t)))$, and $\Phi_q = \mathscr{F}(\phi_0^2(t)\sin(2\psi_\phi(t)))$ are the Fourier transform of the DC, in-phase and quadrature components of the second power of roll. Therefore, by applying the cross-correlation theorem to the signals at hand,

$$\begin{aligned}P_{\phi^2\theta} = \frac{1}{4}\big[&\Phi_i\Theta_i(\omega-2\omega_\phi)+\Phi_i\Theta_i(\omega+2\omega_\phi)+\Phi_q\Theta_q(\omega-2\omega_\phi)\\ &+\Phi_q\Theta_q(\omega+2\omega_\phi)-\Phi_i\Theta_q(\omega-2\omega_\phi)-\Phi_i\Theta_q(\omega+2\omega_\phi)\\ &-\Phi_q\Theta_i(\omega-2\omega_\phi)-\Phi_q\Theta_i(\omega+2\omega_\phi)\big]. \qquad (2.44)\end{aligned}$$

The cross-spectrum is different from zero since $\phi^2(t)$ and $\theta(t)$ are centered at the same frequency; hence the spectral correlation coefficient is different from zero and it can be used for detecting parametric roll.

Consider now a ship sailing in near head seas condition. The lateral component of wave force excites roll motion directly, hence pitch and roll both respond at the same frequency ($\omega_\phi = \omega_\theta = \omega_e$). The cross-spectrum in this case is equal to zero,

$$\begin{aligned}P_{\phi^2\theta} = \frac{1}{4}&\big[\Theta_i(\omega-\omega_e)+\Theta_i(\omega+\omega_e)-\Theta_q(\omega-\omega_e)-\Theta_q(\omega+\omega_e)\big]\\ &\times\big[\Phi_0(\omega)+\Phi_i(\omega-2\omega_e)+\Phi_i(\omega+2\omega_e)\\ &-\Phi_q(\omega-2\omega_e)-\Phi_q(\omega+2\omega_e)\big]=0, \qquad (2.45)\end{aligned}$$

since the spectra are different from zero only around $\omega = \omega_e$ or $\omega = 2\omega_e$. Therefore the spectral correlation coefficient is zero, showing that the proposed detection method is insensitive to forced roll.

The GLRT for the Weibull distribution of the local minima $z(k)$ is also proven to be insensitive to forced roll. Consider pitch and roll as sinusoidal signals:

$$\theta(t) = \theta_0\cos(\omega_\theta t+\varsigma) \qquad (2.46)$$

$$\phi(t) = \phi_0\cos(\omega_\phi t). \qquad (2.47)$$

In forced roll condition, roll and pitch are sinusoids of the same frequency ($\omega_\theta = \omega_\phi = \omega$), which yields the following driving signal:

$$\begin{aligned} d(t) &= \phi^2(t)\theta(t) \\ &= \phi_0^2\theta_0 \cos^2(\omega t)\cos(\omega t + \varsigma). \end{aligned} \tag{2.48}$$

According to (2.25) we have that

$$z(k) = \alpha(\varsigma)\phi_0^2\theta_0 \leq \phi_0^2\theta_0, \quad 0 < \alpha(\varsigma) \leq 1, \tag{2.49}$$

where $\alpha(\varsigma)$ is the amplitude reduction factor due to the phase shift between the two wave forms.

To prove that the GLRT detector is not sensitive to forced roll, we need to demonstrate that there exists a constant Γ such that for any $\gamma > \Gamma$ the detector does not trigger an alarm. In general Γ is function of the phase shift ς and of the time interval ΔT over which the estimates of the scaling and shape factors are performed. In particular the time interval ΔT determines how many local minima are taken into account for the detection.

To find Γ we need to prove that

$$(\beta_1 - \beta_0)\sum_{k=1}^{N}\log z(k) - \frac{1}{\upsilon_1^{\beta_1}}\sum_{k=1}^{N} z(k)^{\beta_1} + \frac{1}{\upsilon_0^{\beta_0}}\sum_{k=1}^{N} z(k)^{\beta_0} \tag{2.50}$$

is upper bounded. For any $\Delta T \in [0\ ,\ T]$, where $T = 2\pi/\omega$ is the natural roll period, the GLRT detector is not sensitive to forced roll if the threshold γ is set larger than

$$\Gamma \triangleq N_{\max}(\beta_1 - \beta_0)\log(\phi_0^2\theta_0) - \frac{N_{\max}}{\upsilon_1^{\beta_1}}(\phi_0^2\theta_0)^{\beta_1} + \frac{N_{\max}}{\upsilon_0^{\beta_0}}(\phi_0^2\theta_0)^{\beta_0}, \tag{2.51}$$

where $N_{\max}$ is the maximum number of local minima, which fall within one roll period.

2.4 Detection System Robustification

The proposed detection schemes rely on assumptions, which in general may not be completely fulfilled during real navigation operations. The spectral correlation performs best when the signals at hand have a narrow band power spectrum because in that case the Fourier transform of the convolution between the second power of roll with pitch will be zero most of time except when parametric roll is developing. However, in real sailing conditions the wave spectrum exciting the ship motions can be rather large, and it induces ship responses whose frequency content spans over a wide range of frequencies as well. Figure 2.7 compares the power spectra of time series recorded during an experiment in a towing tank, and during a container vessel voyage through an Atlantic storm.

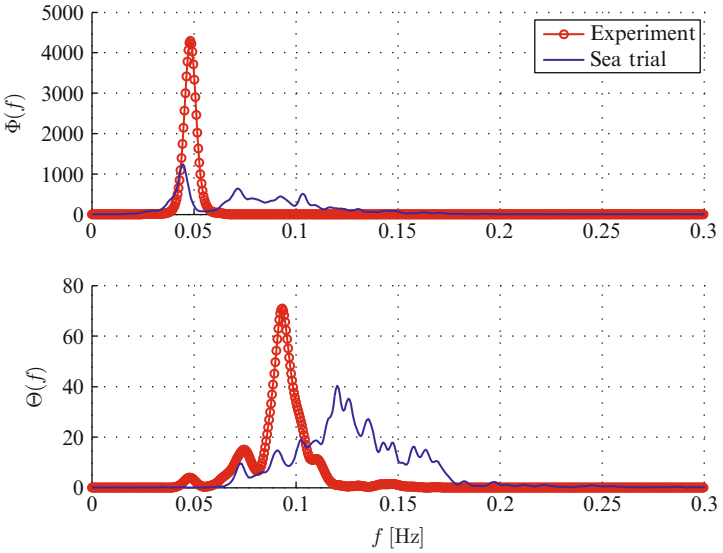

Fig. 2.7 Comparison of power spectra for model basin and Atlantic storm

During real navigation, the roll and pitch motions have an energy content different from zero over a wide range of frequencies, and this will contribute to determine a nonzero spectral correlation also in these regions of frequencies where parametric roll is not likely. Consequently robustification of the spectral correlation is needed.

This is obtained by bandpass filters that narrow in the roll and pitch signals frequency ranges of interest. The pass-bands regions are centered about ω_ϕ and $\omega_e = 2\omega_\phi$, to focus on frequency ranges where parametric roll resonance can develop. The spectral correlation hence takes the form

$$ {}^{f}\mathscr{S}_{\phi^2\theta} = \frac{{}^{f}\sigma^2_{\phi^2\theta}}{\sqrt{\sigma^2_{\phi^2}\sigma^2_{\theta}}}, \tag{2.52} $$

where the superscript f addresses that the computation involves the filtered signals. The normalization factor in (2.52) is still calculated from the raw roll and pitch signals.

For the phase condition (GLRT) detector, a time-varying scaling factor $\lambda(t)$ is applied to the driving signal in (2.24) to adapt to weather conditions. Furthermore, the $\mathscr{H}_0$ parameters are estimated on-line. These together served to obtain desired false alarm rates and make the GLRT detector insensitive to changes in sea state. Assume that we are at time $t = T$ and the GLRT is fed with data logged within the window $[T - M + 1, T]$. The scaling factor λ is computed taking into account all the data from the time window $[T - n * M + 1, T - M]$, where $n \in \mathbb{N}$ is a design parameter.

Utilizing the $\mathscr{W}$-GLRT detector we should assume that the Weibull PDFs for the nonresonant and resonant case differ both for the shape β and scale υ parameters. In Sect. 2.3.2.2 it was shown that the MLE of the shape parameter is found as a solution of a nonlinear equation, which in practice must be solved at each iteration of the algorithm. However, data show that the shape factor remains approximately unchanged, hence, $\beta_0 = \beta_1 = \beta$. Therefore, the $\mathscr{W}$-GLRT detector only looks for variations in the scale parameter υ.

Finally, it is important to point out how the thresholds were chosen. For the cross-correlation, the spectral correlation coefficient ${}^{f}\mathscr{S}_{\phi_2\theta}$ varies between zero and one, hence the threshold $\bar{\mathscr{T}}$ can be set to any value higher than 0.4 according to how conservative the detector should be.

For the GLRT-based detector it was shown that an empirical threshold can be computed based on the estimated $\mathscr{H}_0$ distribution of the test quantity $g(k)$.

2.5 Detection Scheme Validation

This section presents the validation of the detection schemes on both model scale and full scale data sets. After introducing the data sets, the performance of the Weibull GLRT detector is evaluated in both scenarios. Next, the overall robust performance of the monitoring system given by the integration of the spectral correlation detector with the $\mathscr{W}$-GLRT detector is tested. For the performance assessment of the spectral correlation detector the reader may refer to [14].

2.5.1 Experimental and Full Scale Data Sets

To assess the performance of the proposed detection schemes for parametric roll the detectors have been validated against two data sets. The first data set consists of eight experiments run in irregular waves scenario.[2] The vessel used for the experiments was a 1:45 scale model of a container ship with length overall of 294 m. The principal dimensions and hydrodynamic coefficients can be found in [18]. The time-history of roll is shown in Fig. 2.9 (top plot). Although the vessel experienced parametric roll only once, all the experiments were made to trigger the resonant phenomenon, but in the irregular wave scenario it is somewhat difficult to obtain a fully developed parametric roll resonance, because consecutive wave trains may not fulfill all conditions for its development.

[2]The terminology irregular wave scenario means that the wave motion used to excite the vessel is generated by the interference of multiple sinusoidal waves centered at different frequencies, and it is described by a given power spectrum. This terminology is used in opposition to the regular wave scenario where instead the vessel is excited by a single sinusoidal wave.

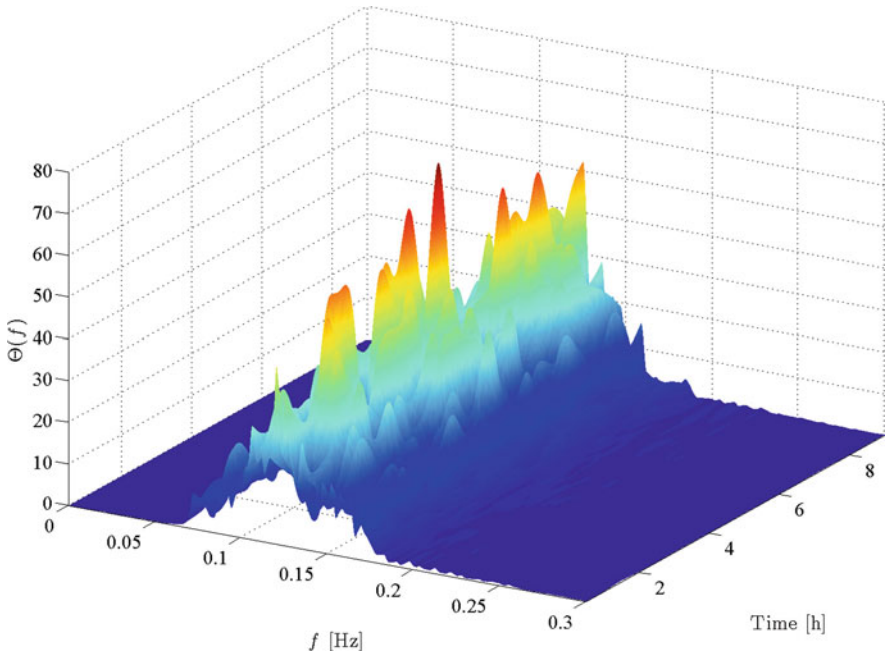

Fig. 2.8 The evolution of the pitch power spectrum provides an idea of the frequency content of the wave spectrum during the navigation

The second data set is full scale data recorded on board Clara Maersk, a 33000 dwt container ship crossing the North Atlantic. Nine hours of navigation were analyzed. Conditions were significant wave height judged by navigators to develop from 5–6 m to 7–10 m. Relative direction of waves were 150°–170° where 180° is head sea. The pitch power spectrum shown in Fig. 2.8 provides an idea of the broad frequency content of the wave spectrum exciting the container ship during the storm.

For this data set it is essential to point out that there was no prior awareness about the onset of parametric roll resonance; hence the assessment of detections and/or false alarms was done by visual inspection of the time series around the alarm time.

The model test experimental data set is used to evaluate the capability of the detectors to timely catch the onset of parametric roll; whereas the real navigation data set is used to ensure the insensitivity to usual forced roll.

In order to simulate a continuous navigation the single records of the two data set have been stitched together. A smoothing filter was applied around the stitching points to avoid that sudden fictitious variations within the signals at hand could trigger an alarm. Hence the roll time series scrutinized are those shown in Fig. 2.9.

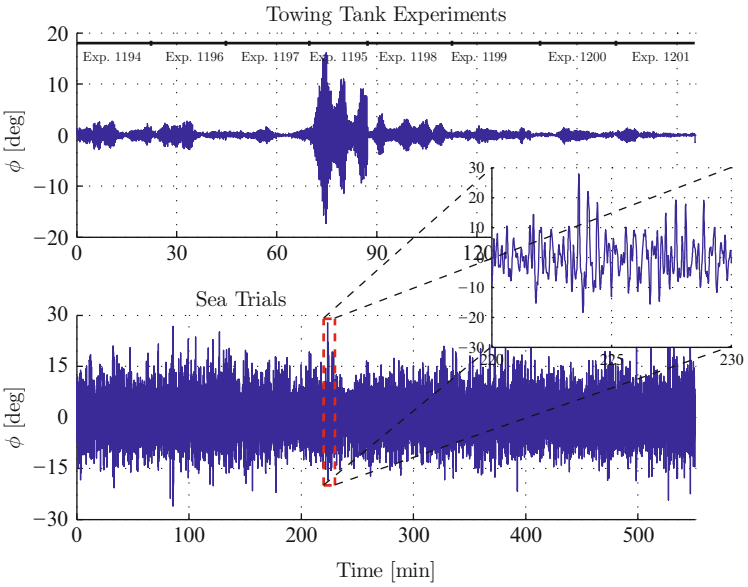

Fig. 2.9 *Top*: Roll motion time series recorded from experimental runs. Experiment 1195 is the only one where parametric roll clearly developed. *Bottom*: Roll motion time series recorded during navigation across the North Atlantic Ocean

2.5.2 *Validation of Weibull GLRT Detector*

Figures 2.10 and 2.11 show the results of the Weibull GLRT detector after processing the model and full scale data sets.

On the experimental data set the Weibull GLRT detector performs well. Figure 2.10 illustrates that the parametric roll event that occurs between $t = 70$ min and $t = 90$ min is timely detected when the roll angle is about 3°. The lost of phase synchronization is also detected by the Weibull GLRT, which withdraws the alarm at $t = 90$ min when the roll motion decays and it seems that the parametric resonance is over. However, a new alarm is suddenly raised when the resonant oscillations take place again.

On the sea trial data set the Weibull GLRT detector raises five alarms, which all last for exactly one window length M, as shown in Fig. 2.11. Since no prior awareness about the presence/absence of parametric roll events was available for this data set, the alarms have been classified by visual inspection and it was concluded that all five cases are likely to be false alarms.

It is not surprising that a single detector cannot provide full information about the resonance condition since both the phase synchronization and the frequency coupling must be satisfied simultaneously. Robust detection performance therefore needs simultaneous detection of the presence of both conditions.

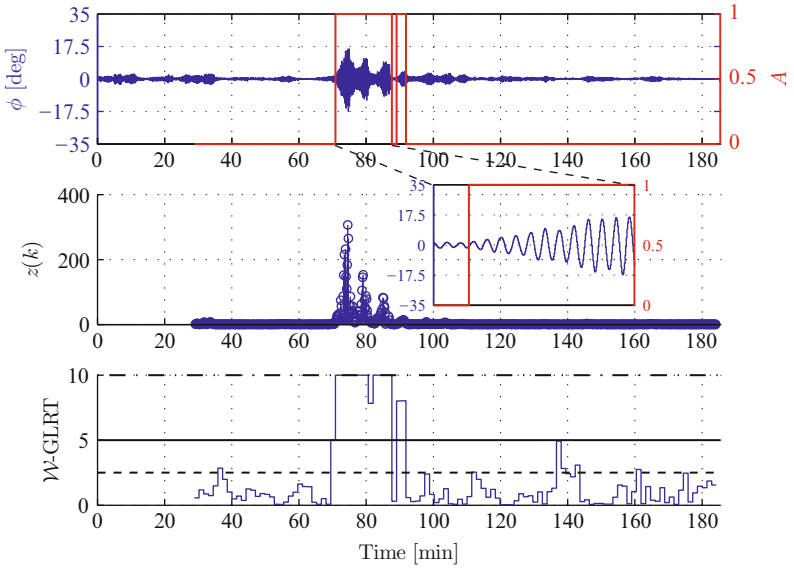

Fig. 2.10 Weibull GLRT detector on the experimental data set: the onset of the parametric roll event is timely detected when the roll angle is only about 3°

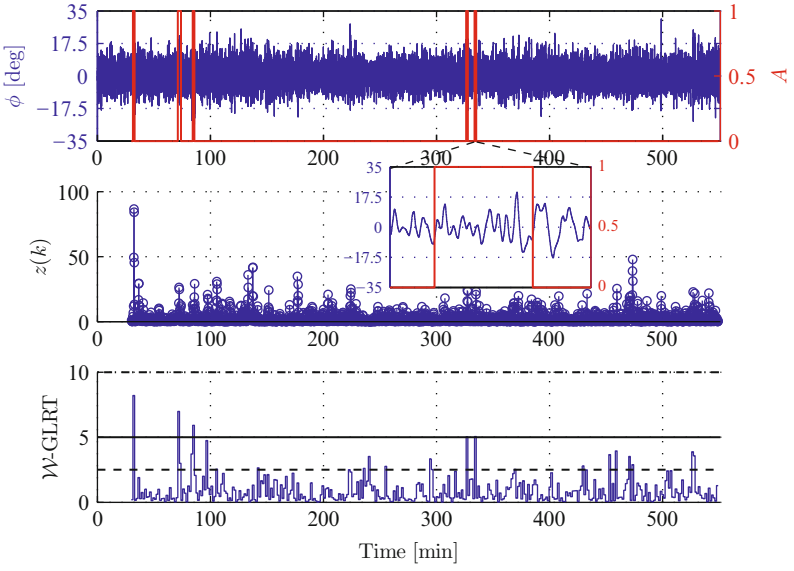

Fig. 2.11 Weibull GLRT detector on the sea trial data set: the detector raises five alarms. Visual inspection of the alarm cases suggests that those are false alarms

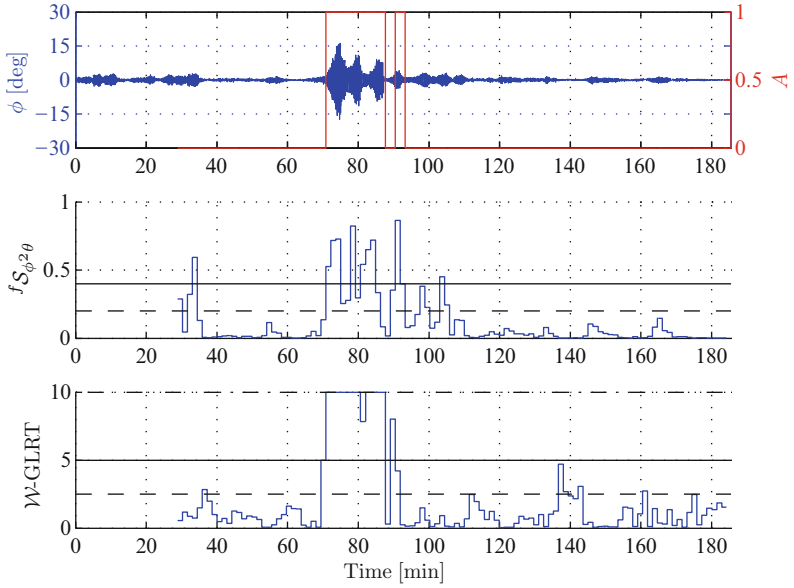

Fig. 2.12 Performance of the monitoring system on the model basin experimental data set

2.5.3 Robust Performance

The spectral correlation detector and the Weibull GLRT detector have shown fairly good performance providing a timely detection but they both give false alarms. To obtain the full picture, the two detectors are combined within a monitoring system, which issues alarms of parametric roll occurrence based upon the tests made by both detectors together. Furthermore, robustness is obtained by making the adaptation to prevailing conditions only when none of the thresholds are exceeded. This means the $\mathscr{H}_0$ statistics and the normalization of the spectral correlation in practice are calculated from data that are older than the data windows used – a few roll periods – and with appropriate forgetting to be able to track changes in weather. The performance of the monitoring system with robustified algorithms is shown in Fig. 2.12 for the model basin experimental data set, and in Fig. 2.13 for the real navigation data. The general quality of detection performance is apparent.

The performance improvement of the Weibull GLRT detector when combined with the spectral correlation detector is shown in Fig. 2.13. The reduction of false alarms is determined by the fact that in this case the update of the scaling factor $\lambda(t)$ is related to the alarms raised by the monitoring system and not to those issued by the Weibull GLRT detector alone.

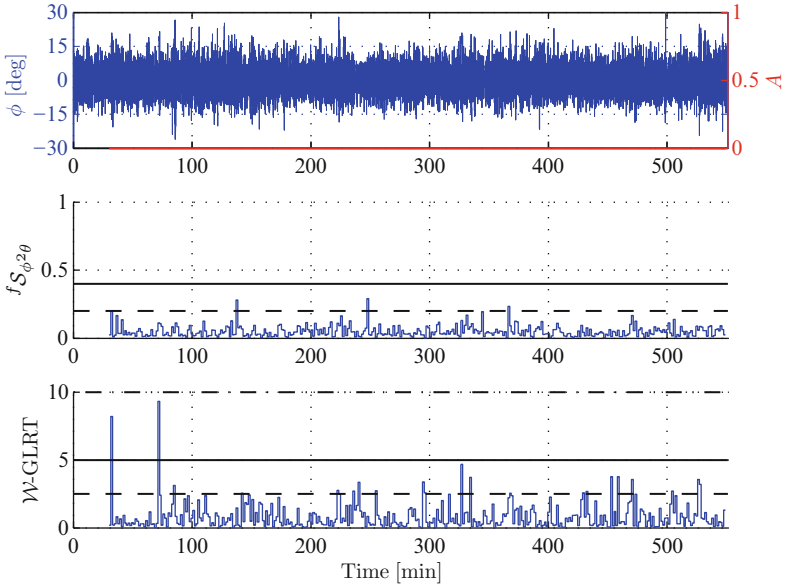

Fig. 2.13 Performance of the monitoring system on navigation data from Clara Maersk

2.5.4 Discussion

While the results have shown very convincing from model tank testing where parametric resonance was present and Atlantic passage in a storm, where it was believed, but not known with certainty that no parametric resonance was present, an independent test with full-scale data would be needed for final proof of the concepts and algorithms presented in this chapter. Such data have recently been made available from trials where also wave radar data were logged. The results with these data were convincing but this validation is outside the scope and space allocated to this chapter. The monitoring system methodology and implementation are patent pending [11], and is expected to find its way to the Seven Seas under the trade mark *PAROLL*®.

2.6 Conclusions

Detection methods were investigated for the diagnosis of parametric roll resonance and were validated against data from model basin tests and from a full-scale Atlantic crossing with a container vessel.

In the spectral domain, spectral analysis provided an indicator for energy flowing from the pitch motion, directly excited by the waves, into roll motion causing resonance. In the time domain, a Weibull GLRT detector monitored the behavior

of a driving signal carrying information about the phase correlation between the square of the roll angle and the pitch angle. Robustness against usual forced roll motion was shown for both detectors.

The detectors showed to be very capable of timely detecting the onset of parametric roll, while achieving a very low false alarm rate. A necessary part of achieving excellent overall detection performance was obtained by combining the hypotheses from the two detectors.

Acknowledgements The authors are grateful for financial support from DTU for the *Proof of Concept* project *PAROLL*. The invaluable collaboration and comments from Dr. G. Storhaug and colleagues from Det Norske Veritas are gratefully acknowledged, and so is the inspiring collaboration and discussions with colleagues at the CeSOS center of excellence at NTNU. Data from model tests were kindly provided by Dr. Perez (formerly CeSOS, NTNU now Univ. of Newcastle, AUS) and Dr. Storhaug, DNV. Data from the Atlantic passage were logged by M. Blanke in the 1980s and are presented here with the permission from the owner, Maersk Lines. The help received from Mr. T. Krarup Sørensen from Maersk and the officers and crew of Clara Maersk in organizing and conducting the sea tests are much appreciated.

References

1. Balakrishnan, N., Kateri, M.: On the maximum likelihood estimation of parameters of weibull distribution based on complete and censored data. *Statistics and Probability Letters*, 78: 2971–2975 (2008).
2. Basseville, M., Nikiforov, I. V.: *Detection of Abrupt Changes: Theory and Applications*. Prentice Hall (1993).
3. Belenky, V., Yu H., Weems, K.: Numerical procedures and practical experience of assessment of parametric roll of container carriers. In *Proceedings of the 9th International Conference on Stability of Ships and Ocean Vehicles*. Brazil (2006).
4. Blanke, M., Kinnaert, M., Lunze, J., Staroswiecki, M.: *Diagnosis and fault-tolerant control* 2nd edition, Springer, Germany (2006).
5. Bulian, G., Francescutto, A., Umeda, N., Hashimoto, H.: Qualitative and quantitative characteristics of parametric ship rolling in random waves. *Ocean Engineering*, 35:1661–1675 (2008).
6. Carmel, S. M.: Study of parametric rolling event on a panamax container vessel. *Journal of the Transportation Research Board*, 1963:56–63 (2006).
7. Døhlie, K. A.: Parametric rolling – a problem solved? *DNV Container Ship Update*, 1:12–15 (2006).
8. France, W. N., Levadou, M., Treakle, T. W., Paulling, J. R., Michel, R. K., Moore, C.: An investigation of head-sea parametric rolling and its influence on container lashing systems. In: *SNAME Annual Meeting*. SNAME Marine Technology 40(1):1–19 (2003).
9. Froude, W.: On the rolling of ships. *Transactions of the Institution of Naval Architects*, 2: 180–227 (1861).
10. Froude, W.: Remarks on Mr. Scott Russel's paper on rolling. *Transactions of the Institution of Naval Architects*, 4:232–275 (1863).
11. Galeazzi, R., Blanke, M., Poulsen, N. K.: Prediction of resonant oscillation, EP09157857, filed April 2009 (2009).
12. Galeazzi, R., Blanke, M., Poulsen, N. K.: Detection of parametric roll resonance on ships from indication of nonlinear energy flow. In: *Proceedings 7th IFAC Symp. on Fault Detection, Supervision and Safety of Technical Processes*. IFAC, Spain (2009).
13. Galeazzi, R., Blanke, M., Poulsen, N. K.: Parametric roll resonance detection using phase correlation and log-likelihood testing techniques. In: *Proceedings of the 8th IFAC International Conference on Manoeuvring and Control of Marine Craft*. IFAC, Brazil (2009).

14. Galeazzi, R., Blanke, M., Poulsen, N. K.: Early detection of parametric roll resonance on container ships. *Technical report, DTU Electrical Engineering, Technical University of Denmark* (2011).
15. Ginsberg, S.: Lawsuits rock APL's boat – Cargo goes overboard; insurance lawyers surface (1998).
16. Grimshaw, R.: *Nonlinear ordinary differential equations*. CRC Press, United States of America (1993).
17. Hashimoto, H., Umeda, N.: Nonlinear analysis of parametric rolling in longitudinal and quartering seas with realistic modeling of roll-restoring moment. *Journal of Marine Science and Technology*, 9:117–126 (2004).
18. Holden, C., Galeazzi, R., Rodríguez, C., Perez, T., Fossen, T. I., Blanke, M., Neves, M. A. S.: Nonlinaer container ship model for the study of parametric roll resonance. *Modeling, Identification and Control*, 28:87–113 (2007).
19. Holden, C., Perez, T., Fossen, T. I.: Frequency-motivated observer design for the prediction of parametric roll resonance. In: *Proceedings of the 7th IFAC Conference on Control Applications in Marine Systems*. IFAC, Croatia (2007).
20. Jensen, J. J.: Efficient estimation of extreme non-linear roll motions using the first-order reliability method (FORM). *Journal of Marine Science and Technology*, 12:191–202 (2007).
21. Jensen, J. J., Pedersen, P. T., Vidic-Perunovic, J.: Estimation of parametric roll in stochastic seaway. In: *Proceedings of IUTAM Symposium on Fluid-Structure Interaction in Ocean Engineering*. Springer, Germany (2008).
22. Kay, S. M.: *Fundamental of statistical signal processing vol II: detection theory*. Prentice Hall, United States of America (1998).
23. Kerwin, J. E.: Notes on rolling in longitudinal waves. *International ShipBuilding Progress*, 2(16):597–614 (1955).
24. Levadou, M., Palazzi, L.: Assessment of operational risks of parametric roll. In: *SNAME Annual Meeting*. SNAME, United States of America (2003).
25. McCue, L. S., Bulian, G.: A numerical feasibility study of a parametric roll advance warning system. *Journal of Offshore Mechanics and Arctic Engineering*, 129:165–175 (2007).
26. Nayfeh, A. H., Mook, D. T.: *Nonlinear Oscillations*. WILEY-VCH, Germany (2004).
27. Neves, M. A. S., Rodriguez, C. A.: A coupled third order model of roll parametric resonance. In C. Guedes Soares, Y. Garbatov, and N. Fonseca, editors, *Maritime Transportation and Exploitation of Ocean and Coastal Resources*, pp. 243–253. Taylor & Francis (2005).
28. Neves, M. A.S., Rodriguez, C. A.: On unstable ship motions resulting from strong non-linear coupling. *Ocean Engineering*, 33:1853–1883 (2006).
29. Newman, J. N.: *Marine Hydrodynamics*. The MIT Press, United States of America (1977).
30. Nielsen, J. K., Pedersen, N. H., Michelsen, J., Nielsen, U. D., Baatrup, J., Jensen J. J., Petersen, E. S.: SeaSense - real-time onboard decision support. In: *World Maritime Technology Conference* (2006).
31. Oh, I. G., Nayfeh, A. H., Mook, D. T.: A theoretical and experimental investigations of indirectly excited roll motion in ships. *Philosophical Transactions: Mathematical, Physical and Engineering Sciences*, 358:1853–1881 (2000).
32. Paulling, J. R., Rosenberg, R. M.: On unstable ship motions resulting from nonlinear coupling. *Journal of Ship Research*, 3(1):36–46 (1959).
33. Shin, Y. S., Belenky, V. L., Paulling, J. R., Weems, K. M., Lin, W. M.: Criteria for parametric roll of large containeships in longitudinal seas. *Transactions of SNAME*, 112 (2004).
34. Spyrou, K. J., Tigkas, I., Scanferla, G., Pallikaropoulos, N., Themelis, N.: Prediction potential of the parametric rolling behaviour of a post-panamax container ship. *Ocean Engineering*, 35:1235–1244 (2008).
35. Tondl, A., Ruijgrok, T., Verhulst, F., Nabergoj, R.: *Autoparametric Resonance in Mechanical Systems*. Cambridge University Press, United States of America (2000).
36. Umeda, N., Hashimoto, H., Minegaki, S., Matsuda, A.: An investigation of different methods for the prevention of parametric rolling. *Journal of Marine Science and Technology*, 13:16–23 (2008).

http://www.springer.com/978-1-4614-1042-3

Parametric Resonance in Dynamical Systems
Fossen, T.I.; Nijmeijer, H. (Eds.)
2012, XIV, 330 p., Hardcover
ISBN: 978-1-4614-1042-3